PHASED-ARRAY ANTENNA CALIBRATION AND CROSS-POLARIZATION IMPROVEMENT OF AN X-BAND WEATHER RADAR

A Thesis Presented

by

GERARD MASALIAS HUGUET

Submitted to Universitat Politècnica de Catalunya
Escola Tècnica Superior d'Enginyeria de Telecomunicació de Barcelona
in partial fulfillment of the requirements for the degree of

ENGINYERIA DE TELECOMUNICACIÓ

October 2015

Electrical Engineering and Computer Science
University of Massachusetts Amherst

PHASED-ARRAY ANTENNA CALIBRATION AND CROSS-POLARIZATION IMPROVEMENT OF AN X-BAND WEATHER RADAR

A Thesis Presented

by

GERARD MASALIAS HUGUET

Approved as to style and content by:

Stephen J. Frasier, Professor
Electrical Engineering and Computer Science

DEDICATION

To my father, mother and sister

ACKNOWLEDGMENTS

I would like to thank all the people who have helped me make this thesis possible.

Thanks to my advisor, professor Stephen Frasier, for giving me the chance to participate in this project. Thanks to Krzysztof for showing me the radar hardware basics. Handling with laboratory instruments could have been a nightmare without Tom, thanks for being so accessible and helpful. I would like to thank Erick for his different points of view and his always brilliant solutions. I do not forget Jack, the chamber guy, I would like to thank him for his guidance and time spent in the anechoic chamber. I cannot thank Sheila enough for being my desk mate, for her talks and for her support way beyond laboratory boundaries. Also, I would like to thank Gerard, I was very lucky to find you here, a big thanks for helping me inside and outside the work, everything would have been much more complicated without you. Eulàlia, thanks for being there everyday and matching my schedules overseas.

Last, but not least, I would like to thank my family. *"Living the dream"* in the U.S. would not have been possible without your constant support and patience. Thanks for everything.

ABSTRACT

PHASED-ARRAY ANTENNA CALIBRATION AND CROSS-POLARIZATION IMPROVEMENT OF AN X-BAND WEATHER RADAR

OCTOBER 2015

GERARD MASALIAS HUGUET

UNIVERSITY OF MASSACHUSETTS AMHERST

Directed by: Professor Stephen J. Frasier

Dual-polarized phased-array radars used for weather retrieval purposes is an emerging tendency over the last few years. The dual-polarization technology provides an expanded range of weather products and the reliability of these polarimetric produtcs rely on the beam shape quality of the system under use and its polarization isolation.

This thesis presents the calibration process of a one-dimensional scanning phased array radar to assure its beamforming quality. A cross-polarization cancellation technique, with no additional hardware requirements, is tested and appeared to optimize the array settings for an improved isolation and therefore, for a better data quality.

TABLE OF CONTENTS

LIST OF TABLES

Table **Page**

LIST OF FIGURES

Figure **Page**

CHAPTER 1

INTRODUCTION AND MOTIVATION

1.1 Introduction

The Center for Collaborative Adaptive Sensing of the Atmosphere (CASA) has been testing a new concept for a weather radar network as an alternative to the one currently used. This concept is based on a low-cost and low-power dense radar network scanning at low altitudes, up to 3 km [5]. Higher density should counteract the lower power and lower altitudes should provide more accurate weather data.

To obtain a low budget weather radar, the system proposed by [6] [9] and assembled by [7] rely on the fact of using a column-fed phased-array antenna. The column-fed configuration uses solid state amplifers and permits reduction of the number of modules behind the antenna. The phased-array enables to rapid electronic scan in azimuth, providing a refresh rate of less than 1 minute, more than five times faster than current systems and crucial in case of severe weather.

These agile beams produced by the active phased-array have shapes and sidelobe levels dictated by the phase and amplitudes of the radiating elements. The nominal settings of the array are determined through a calibration procedure that accounts for various phases and amplitudes of the microwave components comprising the active array elements. Deviations from these nominal settings affect the beam properties and hence the quality of derived weather products.

1.2 Motivation

The UMass Phase-Tilt Weather Radar (PWTR), an X-band dual-polarization active phased-array, is used to evaluate the calibration stability and accuracy through different methods. Self-diagnostics based on mutual coupling are compared to laboratory-based calibration and near-field antenna chamber measurements. This data will be useful to fully characterize the radar system, guarantee a quality threshold of the beam shapes and correct biases introduced after the calibration. This research may help to improve the radar performance, optimizing the array settings.

In addition, early results of the cross-polarization cancellation technique have already showed promise, encouraging a further development that may provide better performance of such sensitive parameter for the field of study.

CHAPTER 2

PHASED-ARRAY ANTENNA CONCEPTS

A basic single element antenna produces a wide beamwidth and therefore low directivity values due to its small electrical dimension. When narrower beamwidths and higher directivity values are needed, the use of a larger antenna is required. An antenna array is a set of individual antennas connected together combining their amplitudes and phases in such a way as to provide increased performance compared to a single element, and to meet more demanding specifications.

The Array Factor (AF) characterizes the array using the superposition of each element's contribution, as a function of its position and excitation. In a linear array located in the x-y plane and oriented towards z axis, the array factor may be expressed as:

$$AF(\Psi) = \sum_{n=0}^{N-1} a_n \, e^{jn\Psi} \tag{2.1}$$

where n is the element's position on the array, $\Psi = kd\sin(\theta)\cos(\phi) + \alpha$, d is the element spacing of the array elements on the corresponding axis and k is the wavenumber. The AF can also be seen as the Fourier Series of the a_n coefficient. If a progressive phase feeding is used, the excitation coefficient is a complex number that can be expressed as

$$I_n = a_n \, e^{jn\alpha} \tag{2.2}$$

where a_n is the excitation amplitude that can be used as a weighting factor to taper the distribution and α is the excitation progressive phase.

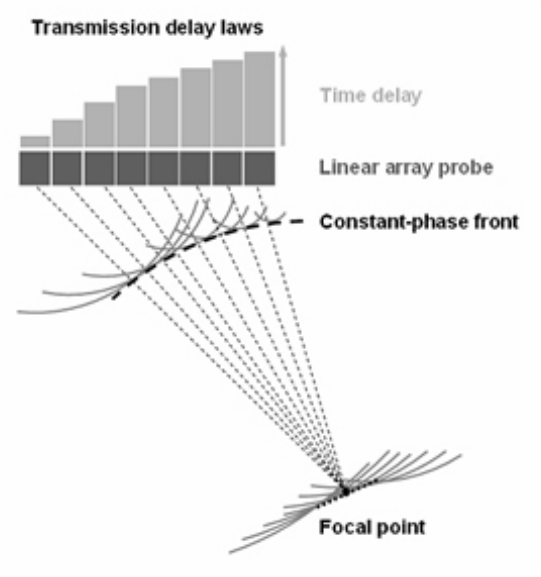

Figure 2.1: Phased Array principles

In Phased Arrays Antennas, if the difference of phases between each element is zero, the direction of the main beam will be broadside. However, if one applies a progressive phase shift, the phase difference α will set the direction of main beam as the offset from the normal of the plane of the antenna. As illustrated in Figure 2.1, a phased array antenna shows its ability to steer the beam direction by shifting the phase. That scanning angle can be calculated by the following equation:

$$\theta_s = \sin^{-1}(\frac{\lambda\ \Delta\psi}{2\pi\ d}) \tag{2.3}$$

where θ_s is the scanning angle, λ is the wavelength, d is the distance between elements and $\Delta\psi$ is the difference of phase between consecutive elements in radians.

The total radiated electric field of an array can be expressed as the single element field by the AF. Using the definition of AF in 2.1 the resultant radiated field is:

$$\vec{E_t}(\vec{r}) = \vec{E_o}(\vec{r})\ AF(\Psi) \tag{2.4}$$

where $\vec{E}_t(\vec{r})$ is the total electric radiated field, $\vec{E}_o(\vec{r})$ is the single element radiated field. The radiation pattern as well, can be deducted from (2.4) as:

$$F_t(\theta, \phi) = F_o(\theta, \phi)\ AF(\theta, \phi) \tag{2.5}$$

CHAPTER 3

SYSTEM DESCRIPTION

3.1 Radar System Overview

The PTWR developed in the Microwave Remote Sensing Laboratory (MIRSL) at the University of Massachusetts is the subject of study in this thesis. The system hardware is described in this chapter, from the transceiver card to the antenna backplane. The principal parameters of the PTWR are shown in Table 3.1 and the RF block diagram is shown in Figure 3.3.

3.1.1 RF system

A transceiver card within the host computer generates the transmitted waveform and samples the received signal at an intermediate frequency of 60 MHz. The transmitted signal uses up to 5 MHz of bandwidth, is shifted to 60 MHz and is converted using a 12-bit D/A converter. The received signal is sampled at 100 MHz using a 14-bit A/D converter and after a shifting, filtering and decimation stage a 16-bit Q&I samples are generated at 6.25 MHz.

These signals go through the up/down converter responsible for converting the transmitted signal at 60 MHz (IF) up to 9.36 GHz (X-band) and the received signal at X-band down to IF. Two local oscillators at 1.7 GHz and 7.6 GHz referenced to a phased locked loop (PLL) at 100 MHz, used as a master clock, comprise the double stage converter (see Figure 3.3). In the transmit chain this architecture provides more than 48 dB of suppression of undesired signals. A loop-back path using a 2-way switch provides real-time control over the RF signal.

Parameter	PTWR
Frequency	9.36 GHz
Beamwidth (az/el)	1.8°-2.6° / 3.6°
Number of T/R modules	64
Polarization	ATAR H,V
Attenuator states	64
Phase shifter states	64
Attenuator step	0.5 dB
Phase step	5.6°
Transmitted power	70 W
Noise floor (B=2MHz)	-106 dBm

Table 3.1: Radar system characteristics of the PTWR

The splitter network is used to feed all the Transmitter/Receiver Modules (TRMs) splitting the signal from the up/down converter into 64, therefore a single signal is fed to each TRM. In the opposite direction, a combiner network coherently adds all the received signals coming from the TRMs to the up/down converter. Each network, as shown in Figure 3.1, is composed of 8 power combiner/dividers. Figure 3.2 shows the inner design of a combiner/divider module: a cascade architecture of Wilkinson power dividers provides a 8-way output.

The TRM has the function to alternate between transmit and receive mode of operation and also has the capability to switch between vertical and horizontal polarization. A low-noise amplifier (LNA) is allocated at the input stage of the receiver channel, and a power amplifier (PA) on the transmitter channel provides more than 1 W. There is a 6-bit attenuator and phase shifter, shared between both channels, to perform the beamforming. The combination of 64 attenuator and phase shifter states each, allows one to control the phase within steps of 5.6° over 360° and the attenuation with a resolution of 0.5 dB within a 31.5 dB dynamic range.

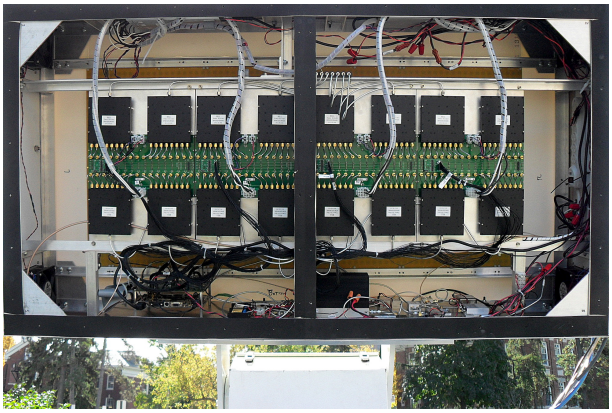

Figure 3.1: PTWR backplane. Upper and lower part black modules conform the splitter network and the combiner network respectively.

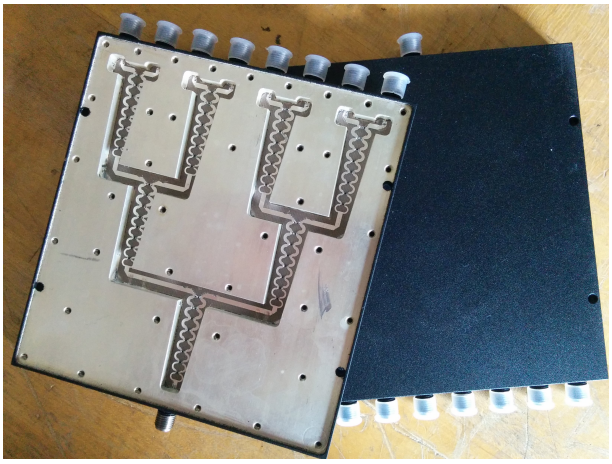

Figure 3.2: Power combiner/divider module. Wilksinon divider is designed using transmission lines.

3.1.2 Hardware Control

A look-up table is generated for each beam, containing the phase shifter and attenuator state for each TRM. A Field Programmable Gate Array (FPGA) formats these settings, generated in the host computer, and stores them together with additional scanning settings such as mode of operation, scan angle or polarization into a sequence table. Finally, the TRM can access the look-up table to upload the settings to its register. A backplane bus interconnects the FPGA with the TRMs and provides

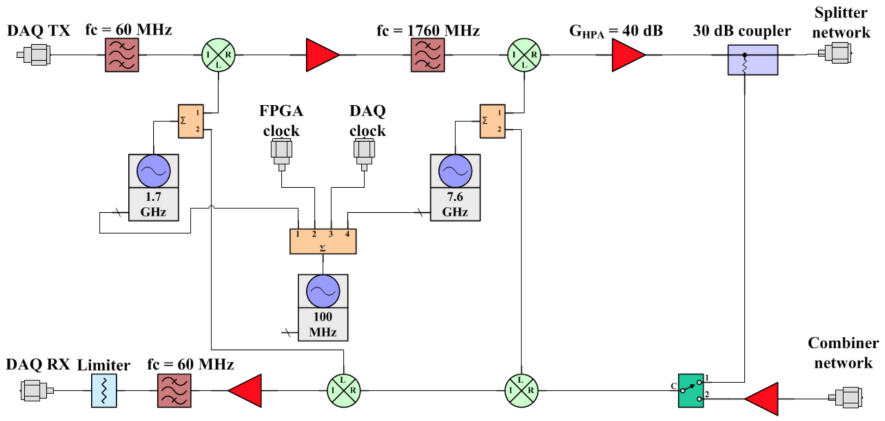

Figure 3.3: Block diagram of the up/down converter

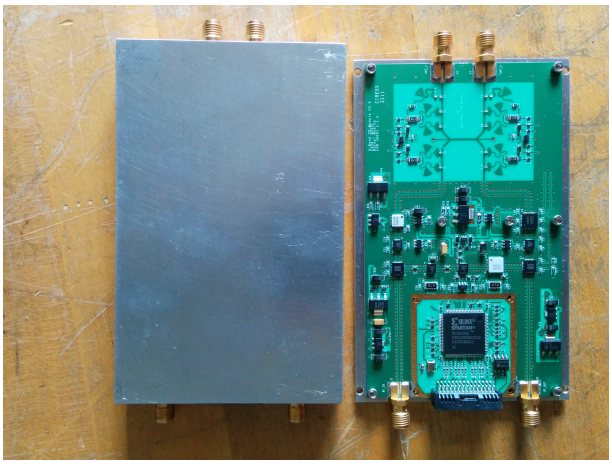

Figure 3.4: Transmitter/receiver module inner PCB. Upper ports are H and V polarizations, lower ports are transmit and receive channels.

the power supply needed for the control signals and for the LNAs and PAs allocated in the TRM gain blocks.

A pedestal is remotely controlled by the computer through a serial interface. A multi-thread control program allows one to synchronize the pedestal elevation angle update with the data acquisition system, once the electronic scan is performed the elevation angle is updated.

3.2 Antenna Description

The array antenna panel consists of 64 active elements (each comprised of 32 individual patches) and additional 8 dummy elements. Each element uses a column-fed configuration that results in a one dimension scanning antenna. It has a modular design composed of 4 panels (see Figure 3.5), making it more scalable in case of a system extension.

3.2.1 Stacked-Patch Configuration

The single embedded element is a square, aperture-coupled microstrip patch antenna using a stacked configuration. Dual polarized fields are obtained through two dog-bone-shaped slot apertures, fed by a sinuous microstrip transmission line. The slots are placed perpendicular to each other, in a T configuration, since it is known to improve the isolation between polarizations [9]. Additionally, a square metal patch located behind the feed helps to reduce the backlobe beam. The radiating element stack-up configuration together with the dielectric materials are shown in Figure 3.6.

3.2.2 Column feeding

The TRM feeds the column antenna using two SMP connectors, one for each polarization. The signal is distributed along the 32 antenna elements using two parallel 100 Ω serpentine feeding lines. In order to feed with the same signal each slot aperture, the line length is computed to provide 360° shift, required between adjacent elements. Quarter-wavelength microstrip sections are used immediately after the port to match the 100Ω. Shown in Figure 3.7, the serpentine feeding line is also used to provide a Taylor taper distribution for a 25 dB sidelobe level.

(a) Rear Panel

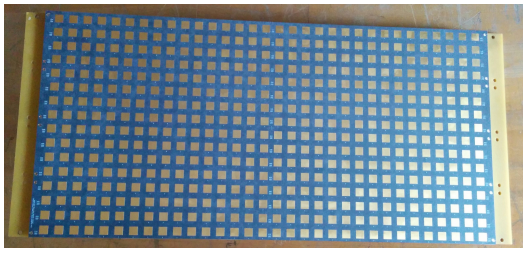

(b) Front panel

Figure 3.5: One of the 4 panels used to assemble the whole array.

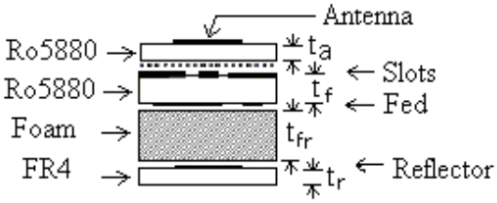

(a) Stack illustration

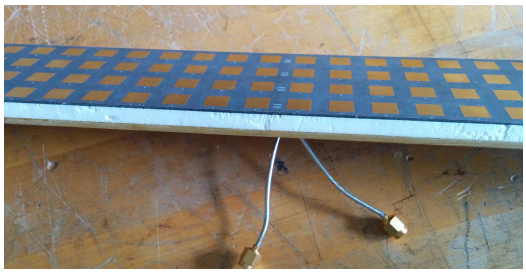

(b) Real printed layers configuration

Figure 3.6: Stacked patch antenna design

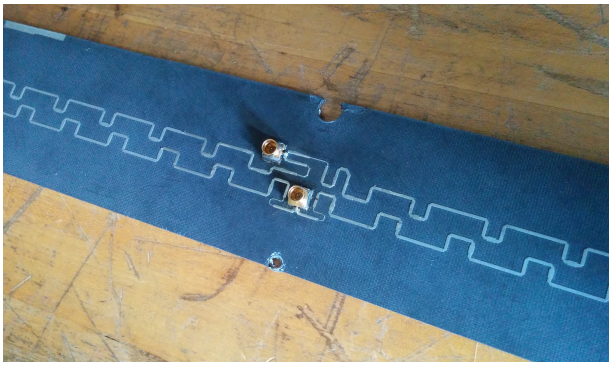

Figure 3.7: Serpentine feeeding line, located between the slot and reflector. H and V ports, upper and lower respectively.

CHAPTER 4

RADAR CALIBRATION

In phased arrays, errors in phase values may result in a beam misalignment, while in amplitude, a poor choice of tapering may affect the sidelobe levels. This chapter describes the fundamentals of calibration, figures of merit and their impact on weather products. It also describes the procedure carried out with the final results.

4.1 Principles of calibration

Calibration consists of measuring a true value, to be able compensate by excess or default, in relation to a nominal value. In a radar system, one can express the received signal in the antenna as [4]:

$$P = C\frac{e^{-2jk_0r}}{4\pi r^2}\mathbf{B^T R^T S_0}(\mathbf{r_0}, \theta_\mathbf{0}, \phi_\mathbf{0})\mathbf{TA} \tag{4.1}$$

where P is the received voltage on the antenna port, $\mathbf{R^T}$ is the overall receive pattern, $\mathbf{S_0}(\mathbf{r_0}, \theta_\mathbf{0}, \phi_\mathbf{0})$ is the back scattering matrix, $\mathbf{T}$ is the overall transmit pattern, $\mathbf{A}$ and $\mathbf{B}^T$ are the transmitted and received voltage vector (H or V) respectively, C is the radar constant and the rest is free space path loss and phase shift. Ignoring the radar constant and the propagation term, the received signal after polarimetric correction at any scan angle can be expressed as:

$$P(r, \theta_s, \phi_s) = \mathbf{B^T C_R R^T}(\theta, \phi, \theta_\mathbf{s}, \phi_\mathbf{s})\mathbf{S}(\mathbf{r}, \theta, \phi)\mathbf{T}(\theta, \phi, \theta_\mathbf{s}, \phi_\mathbf{s})\mathbf{C_T A} \tag{4.2}$$

where $\mathbf{C_R}$ and $\mathbf{C_T}$ are the calibration correction matrices and θ_s and ϕ_s represent a scanning position. Since the goal in any radar application is to measure the back

scattering matrix, the received voltage has to be equal to the back scattered signal. Therefore, one can obtain the following condition:

$$\mathbf{C_R} = \mathbf{R^T}(\theta, \phi, \theta_\mathbf{s}, \phi_\mathbf{s})^{-\mathbf{1}} \tag{4.3}$$

$$\mathbf{C_T} = \mathbf{T}(\theta, \phi, \theta_\mathbf{s}, \phi_\mathbf{s})^{-\mathbf{1}} \tag{4.4}$$

In oder to know how to compensate to achieve the previous condition and simplifying for a one dimension scanning array, the overall patterns can be expressed as:

$$\mathbf{R^T}(\theta, \phi, \theta_\mathbf{s}) = \sum_\mathbf{n} \mathbf{X_n^T}(\theta_\mathbf{s}) \mathbf{R_n^T} \mathbf{F_n^T}(\theta, \phi) \tag{4.5}$$

$$\mathbf{T}(\theta, \phi, \theta_\mathbf{s}) = \sum_\mathbf{m} \mathbf{F_m}(\theta, \phi) \mathbf{T_m} \mathbf{Y_m}(\theta_\mathbf{s}) \tag{4.6}$$

where $\mathbf{T_m}$ and $\mathbf{R_n^T}$ represent the contribution of the TRM element in transmit and receive mode respectively, $\mathbf{X_n^T}(\theta_\mathbf{s})$ and $\mathbf{Y_m}(\theta_\mathbf{s})$ are the element weight for a given scanning angle, and $\mathbf{F_m}(\theta, \phi)$ and $\mathbf{F_n}(\theta, \phi)$ are the element radiation pattern. Thus, by changing the weighting function applied, the calibration procedure should compensate for the differences over different TRMs and polarizations.

4.2 Calibration figures of merit

In addition to biases due to distortions in the RF system, the antenna element itself can also introduce biases and limitations that have to be taken into account in the calibration process. It is critical to characterize the polarization in a dual-pol weather radar, for both phase and amplitude, to delimit the impact on weather products after calibration and to guarantee a quality threshold. Leakage from one polarization when receiving in another will severely affect products depending on the polarimetry, as well as differences in co-polar patterns.

A parameter that accounts for phase and amplitude inequality between two ports is defined in [2] as:

$$\beta_a^2 = \sqrt{\frac{F_h}{F_v}} e^{j(\phi_h - \phi_v)} \tag{4.7}$$

where $F_{h,v}$ is the unnormalized radiation pattern and $\phi_{h,v}$ is the measured phase. Co-polar pattern mismatch can be obtained as the magnitude from (4.7). Then, figures of merit to measure calibration accuracy will be: co-polar pattern mismatch and cross-polarization isolation ratio (CPR). Co-polar pattern mismatches affect directly the Differential Reflectivity (Z_{DR}), hence it can be measured as the Differential Reflectivity bias (Z_{DRb}) as it follows:

$$S = \begin{bmatrix} S_{hh} & S_{hv} \\ S_{vh} & S_{vv} \end{bmatrix} \tag{4.8}$$

$$Z_{DR} = \frac{< |S_{HH}|^2 >}{< |S_{VV}|^2 >} \tag{4.9}$$

the contribution of the antenna radiation pattern to the variable:

$$Z_{DRb} = 10 \log \left(\frac{G_{0h}^2 \iint |i_h^2 + \varepsilon_h^2|^2 \ f_h^2 \ d\Omega}{G_{0v}^2 \iint |i_v^2 + \varepsilon_v^2|^2 \ f_v^2 \ d\Omega} \right) \tag{4.10}$$

where $G_{0h,v}$ is the gain at broadside, $\varepsilon_{h,v}^2$ is the polarization error and $f_{h,v}$ is the normalized radiation pattern. Ideally, from power conservation $i_{h,v}^2 + |\varepsilon_{h,v}|^2 = 1$. Gains can be corrected through calibration and if we assume perfectly matched patterns, then $Z_{DRb} = 0 \ dB$.

4.3 Intrinsic element patterns

The most basic adjustable element in this array configuration is the column, since the TRM feed all 32 elements through the serpentine line. Before any calibration, it is good to characterize the basic element to know the starting point and its constraints. Averaged co-polar pattern mismatches through the 64 columns in each polarization

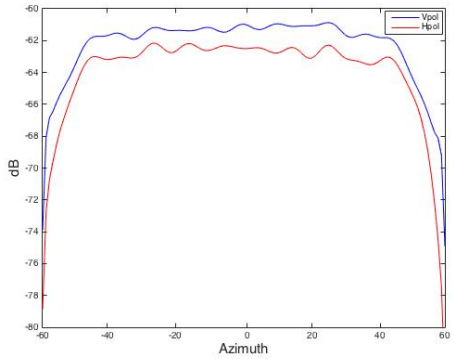

Figure 4.1: F_{hh} and F_{vv} patterns on H plane. Averaged co-polar pattern mismatch for a single column over the 64 TRM. Mismatch(MM)=15.71%.

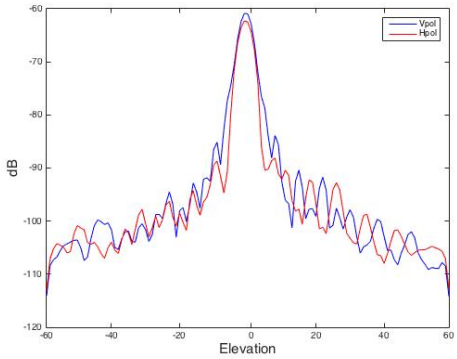

Figure 4.2: F_{hh} and F_{vv} patterns on E plane. Averaged co-polar pattern mismatch for a single column over the 64 TRM. MM=18.4%.

are shown in Figures 4.1 and 4.2, all of them are measured in the near field anechoic chamber. The power decreases as moving away from the column center. This tappering effect on H plane will impact the full array main lobe, decreasing the peak power when scanned away from broadside.

When mismatch is computed over the entire scanned plane, Figure 4.3 shows large differences without calibration, exceeding 4 dB. The reason is that the column itself is already a linear array. Adding the serpentine line effects, yields mismatch that we no have control over. CPR is illustrated in Figures 4.4a and 4.4b, a yellow contour represents where the CPR is better than 20 dB, a required condition in a worst case scenario for an Alternate Transmit Alternate Receive (ATAR) system as defined in [11]. The narrow region, providing barely a couple degrees in elevation, will be very limiting for polarization isolation purposes. 3D column patterns are illustrated in Figure 4.6. The problematic cross-polar shoulders limit the isolation to a narrow region.

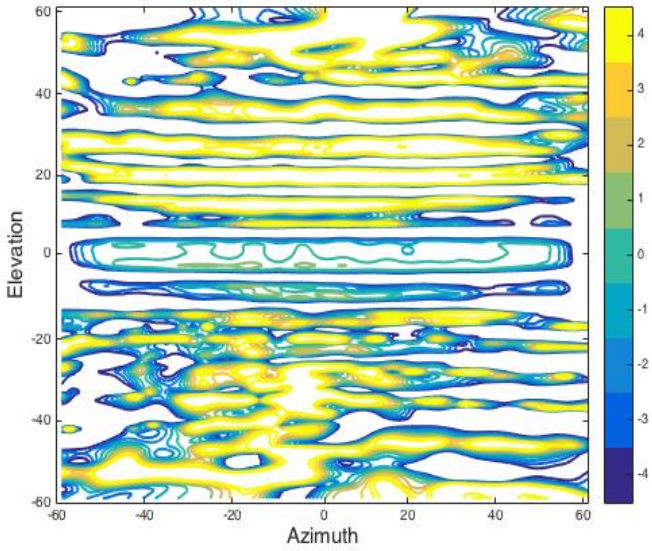

Figure 4.3: F_{hh}/F_{vv} co-polar pattern mismatch over the scanned region. Ideally, on the desired scan range one should have $Z_{DRb} < 0.1$ dB.

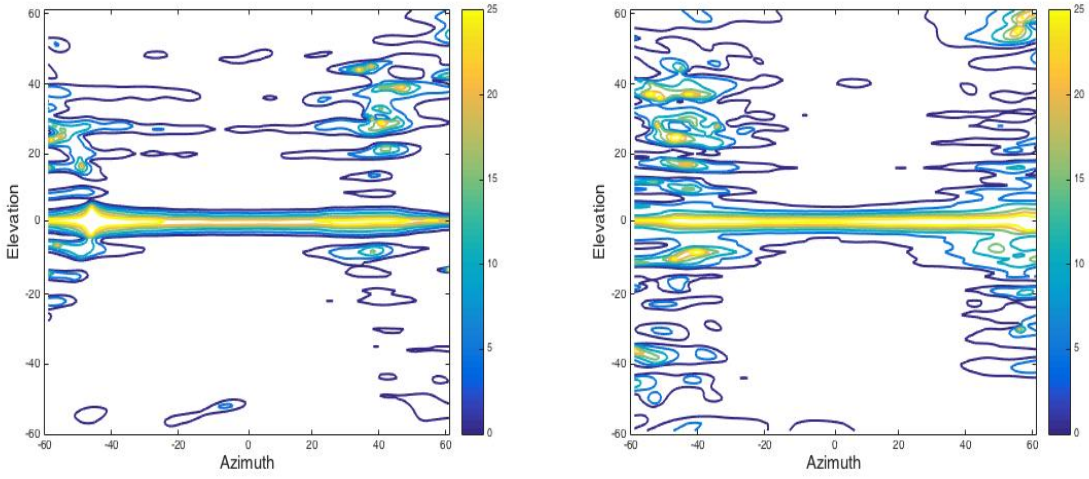

(a) F_{hv} (b) F_{vh}

Figure 4.4: Contour plots for cross-polar patterns for each port, F_{hv} and F_{vh}, over the scanned plane for a single column pattern.

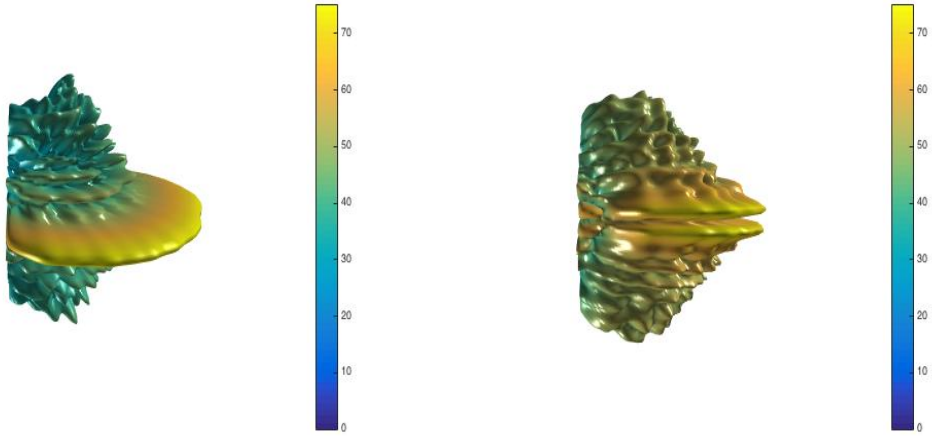

(a) Co-polar pattern

(b) Cross-polar pattern

Figure 4.5: 3D radiation pattern measured from ± 60 degrees on azimuth and elevation. F_{hh} and F_{hv} in a) and b), respectively. Normalized to the lowest value.

4.4 Calibration setup

Different calibration method setups are presented and compared, as well as the calibration procedure. Open End Waveguide Probe (OEWP) and Mutual Coupling (MC) based measurement fundamentals are detailed in this section. External conditions that may distort the measure are also briefly pointed out.

4.4.1 Measurements procedure

The calibration procedure, common in both methods, consists of measuring the antenna S21 parameter using a network analyzer. With a 6-bit attenuator and phase shifter, each TRM offers a combination of 4096 possible states, though a less time-consuming method is used[3]. Instead, 64 attenuator levels are measured keeping phase state to zero, then, 64 phase shifter states are measured with attenuator state set to zero. A matrix with all the possible states can be then obtained through these 128 measurements.

A ”C” language-based code runs the calibration process. The code remotely controlls the network analyzer over ethernet, the OWEP positioner over serial port and updates the array settings through serial port as well (see Figure 4.6). Not more than 32 different states could be uploaded to the TRM registers, thus the measures were taken in sets of 32 each. The code had to be slightly modified to operate in different methods. Once each measurement is done, the network analyzer sends the real and imaginary part of the S21 parameter and it is written into a file.

4.4.2 Mutual coupling and Probe methods

MC involves the interaction of at least two TRM simultaneously, one transmitting and one receiving, since it is essentially measuring the coupling between elements. Several configurations can be applied, using different numbers of TRM in receive or transmit mode, as well as changing position, from nearest neighbors to furthest elements. Usually an external instrument to ”calibrate” one TRM is required, because all measurements are relative to each other, the one used as a reference has to be leveled with an absolute value.

The OEWP method uses a probe located on a positoner, facing the antenna, that moves along the array horizontal axis to measure the different columns as shown in Figure 4.7. The height is adjusted to point exactly at the middle of the column and 2 wavelengths away from the panel.

When calibrating transmit mode, S21 was measured by pulsing the TRMs in both methods, since a 100% duty cycle would have burned them. The differences between signals paths are shown in Figure 4.8. Furthermore, a correction on MC is need to compare the performance of each method side by side. The coupling path, the TRM transmitter channel and the feeding network have to be removed from the raw MC measurements.

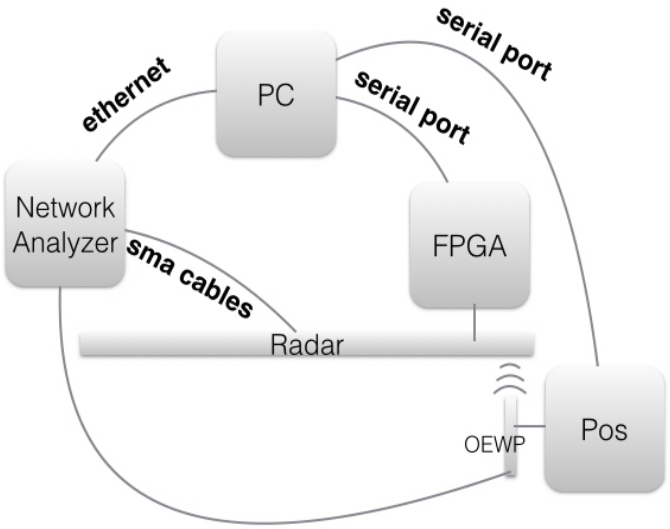

Figure 4.6: Illustration the setup connections and how the host computer interacts with the rest of instruments.

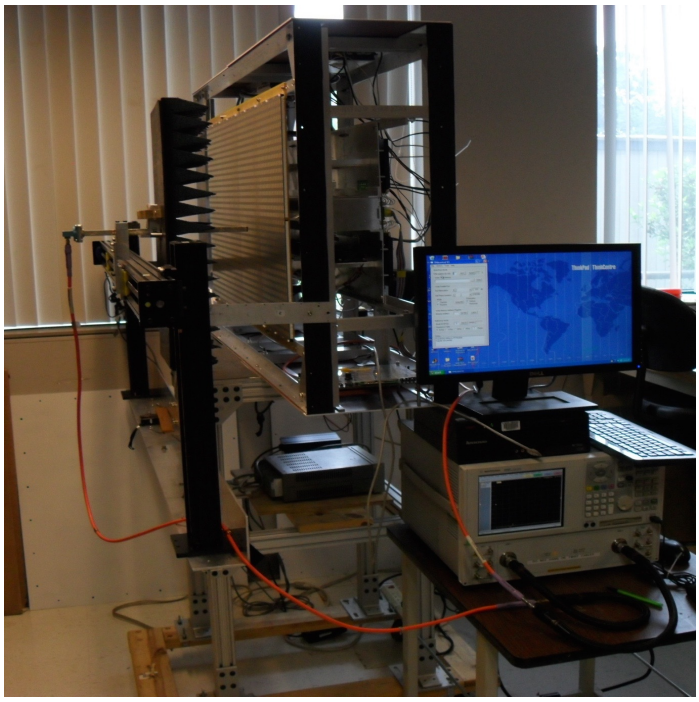

Figure 4.7: Instruments and radar set up for the measurements in the laboratory.

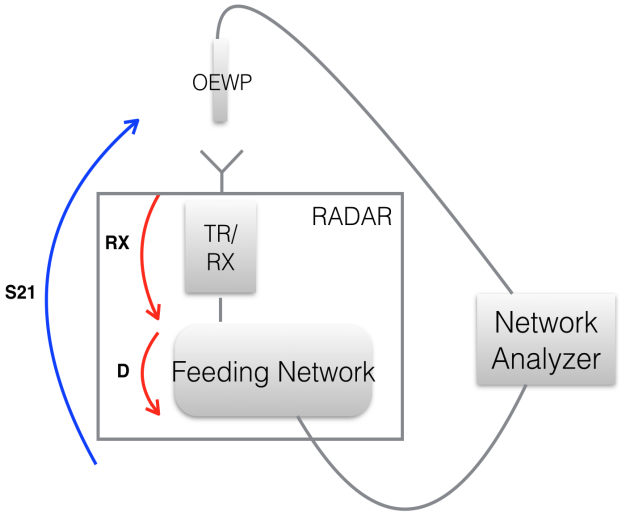

(a) OWEP calibration setup.

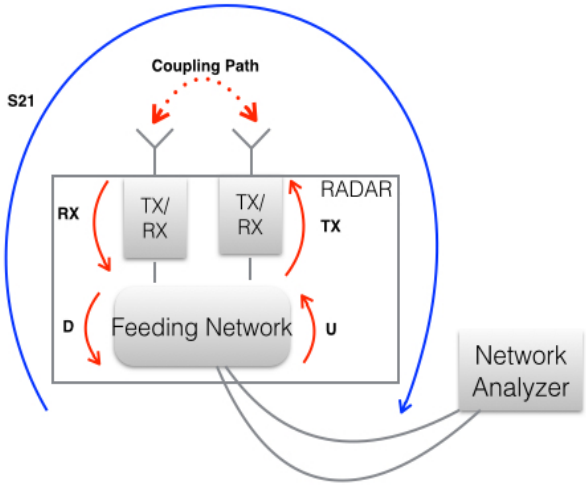

(b) MC calibration setup.

Figure 4.8: Calibration setups illustrate S21 parameter paths. MC uses the radar to transmit and receive the signal whereas in OWEP it is done on separated ends.

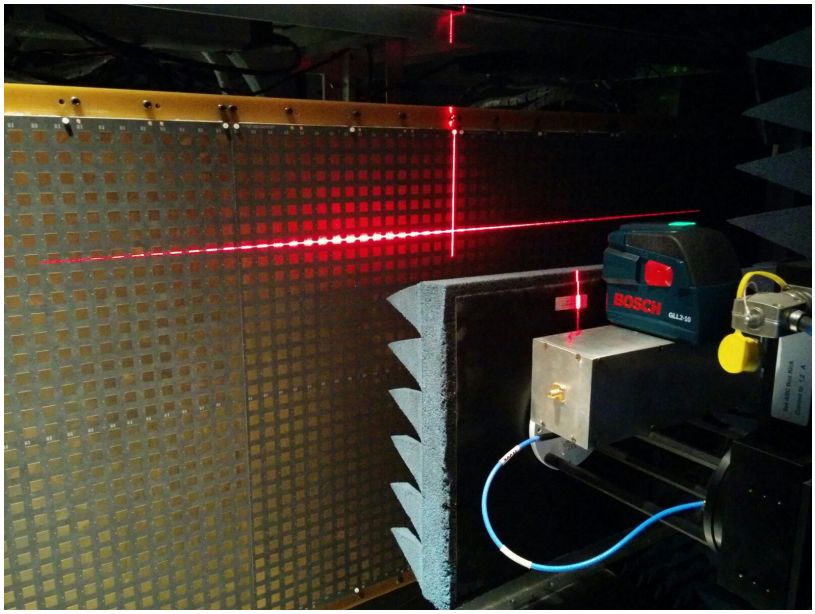

Figure 4.9: Radar and probe alignment in the near field anechoic chamber. A laser was used for a high precision alignment, since cross-polarization measure is really sensitive to small misalignments.

4.4.3 External agents

There is a group of external agents that will affect the reliability of the measurements. Even though we do not have control over some of them, it is good to be aware of their affect and delimit their impact.

Temperature issue has been studied before, and it has been reported a phase drift of 0.7°/C° [7]. It is critical when using transmit mode, specially in closed anechoic chamber, because the TRM will heat up quickly and if the measurements are taken within that time frame, the temperature dependence will severely bias the results. The calibration in the anechoic chamber was done at 42°C±2°C and to mitigate temperature issues the settings sequence in Figure 4.12 was applied.

The positioner's frame was also affecting, specially in the MC method where power is coming out from the antenna panel (see Figure 4.10). To avoid reflections, absorbers foams were placed between the mounted bar and the antenna. In addition, various measures were taken facing different directions to measure how the environment af-

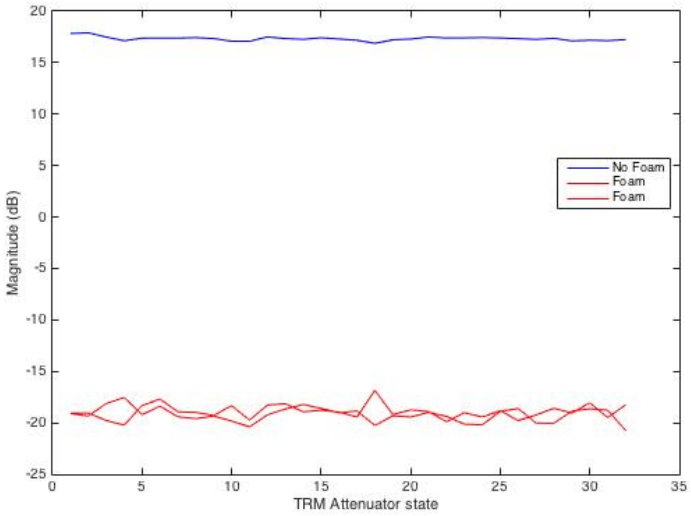

Figure 4.10: Foam effect in measured magnitude when using mutual coupling. More than 30 dB of difference due to the reflections of the metal frame placed in front of the array.

fected inside the laboratory. Figure 4.11 shows that it has a great repeatability, however even the values are consistent over several iterations, this does not guarantee that those are correct. Moreover, the radome (radar cover) characterization was also conducted in the laboratory but inconsistent results and its lack of reliability lead us to discard them as a case of study.

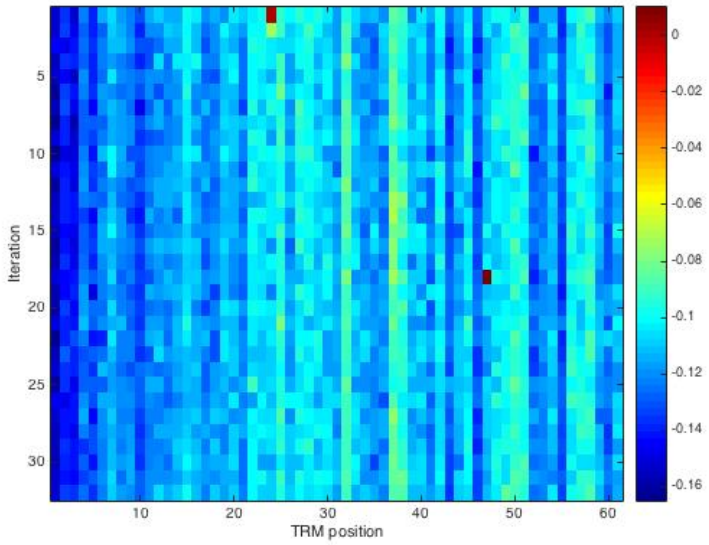

Figure 4.11: Difference in S21 parameter amplitudes. It is measured in dBs, using the same settings over 32 iterations through the 64 TRM and facing different directions in the laboratory.

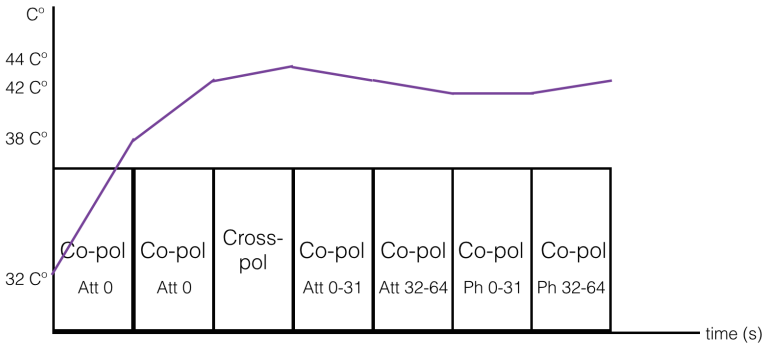

Figure 4.12: Calibration sequence to mitiagate temperature issues on transmit mode. Two unmeasured sets of 32 states transmitting at maximum power heated up the TRM. First measured set is cross-pol, as detailed in chapter 5. Afterwards, co-polar measurements were taken at stable temperature.

4.5 System measurements

Initial pre-calibrated results portray the system condition and how good can it do without calibration. Methods and environments are compared, however OEWP near field chamber results will be the ones used for the radar calibration settings.

The raw magnitude and phase results are shown in Figures 4.13 and 4.14. Few differences are observed in Figures 4.16 a) and b) when comparing laboratory versus anechoic chamber environments using an OWEP. It is notable though, that when approaching to the lower attenuator states, since less power is received, less stable is the measurement. According to Figure 4.15, variations in amplitude up to 3 dB are found when comparing MC based measurements versus OWEP, both conducted in a laboratory environment. Small gaps and irregularities on the panel surface may introduce some distortions on MC. Moreover, the coupling paths do not confine the power as well as an OWEP facing the antenna does. As in the previous comparison, bigger differences are visible at a lower amplitude states together with a line corresponding to state 32 due to the TRM register limitation.

Taking the near field chamber results as a reference, two error vectors associated to each method, for uniformly excited ports, show how intrinsically method and environment errors would affect the beam properties (see Figure 4.20). MC would introduce a misalignment of 1.4° on the main lobe and 1 dB higher sidelobe levels (the first one) when steered to 0° azimuth, whereas OWEP measurement would not affect the beam significantly.

	NF chamber vs Laboratory	MC vs Laboratory
Mean(amp/phase)	0.04 dB/0.21°	0.42 dB/3.63°
Standard Deviation (amp/phase)	0.08 dB/0.46°	0.57 dB/3.47°

Table 4.1: Statistic comparison of methods and environments.

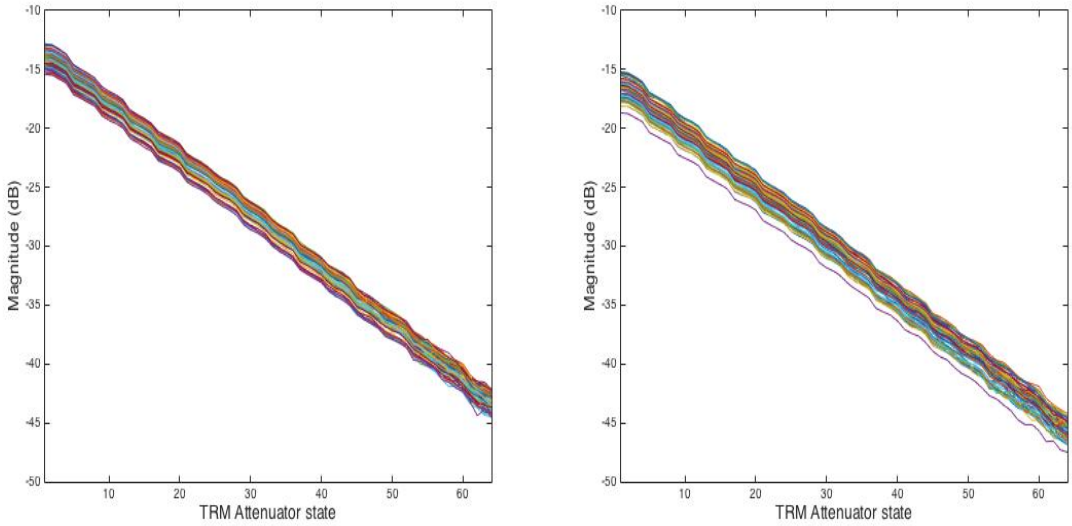

(a) H polarization (b) V polarization

Figure 4.13: Overlapped all TRM measured magnitudes, over 64 attenuator states.

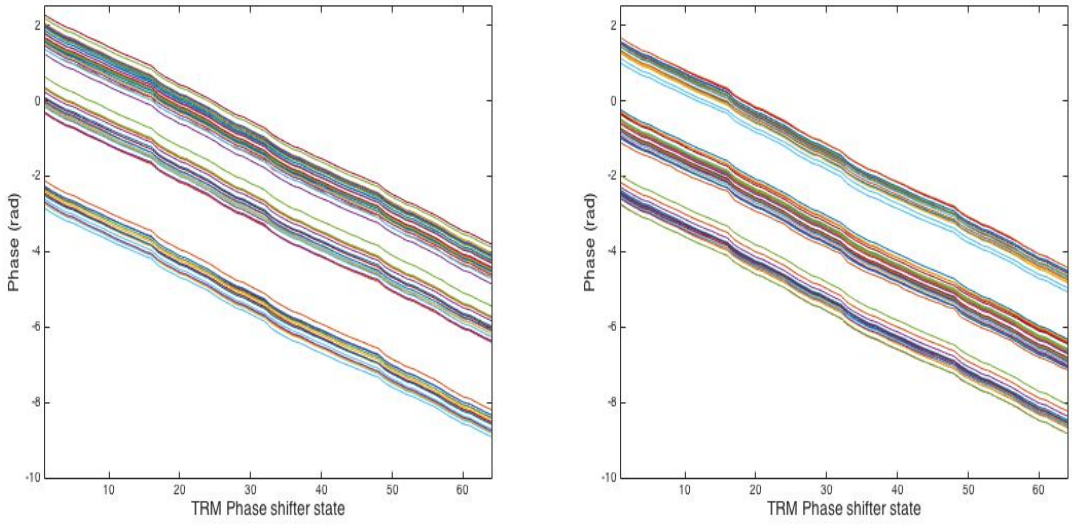

(a) H polarization (b) V polarization

Figure 4.14: Overlapped all TRM measured phases, over 64 phase shifter states.

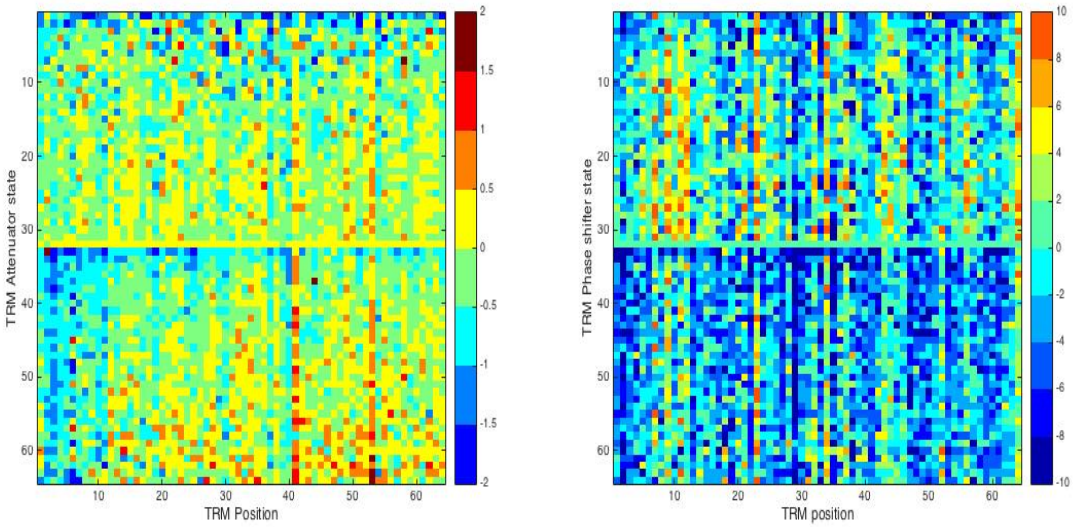

(a) Magnitude difference

(b) Phase difference

Figure 4.15: OWEP and MC methods differences, both performed in a laboratory environment.

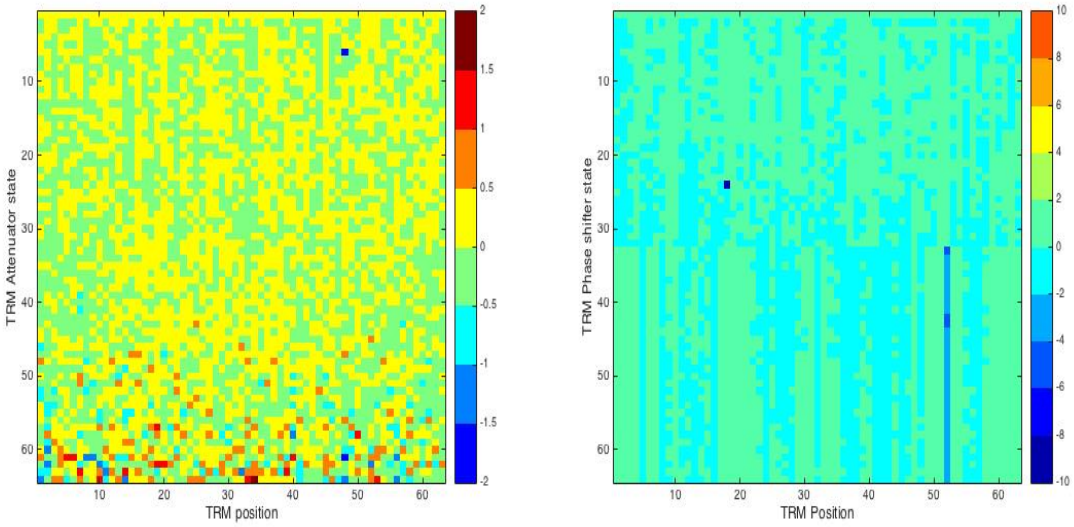

(a) Magnitude difference

(b) Phase difference

Figure 4.16: Near field chamber and laboratory environment differences, both performed using OWEP.

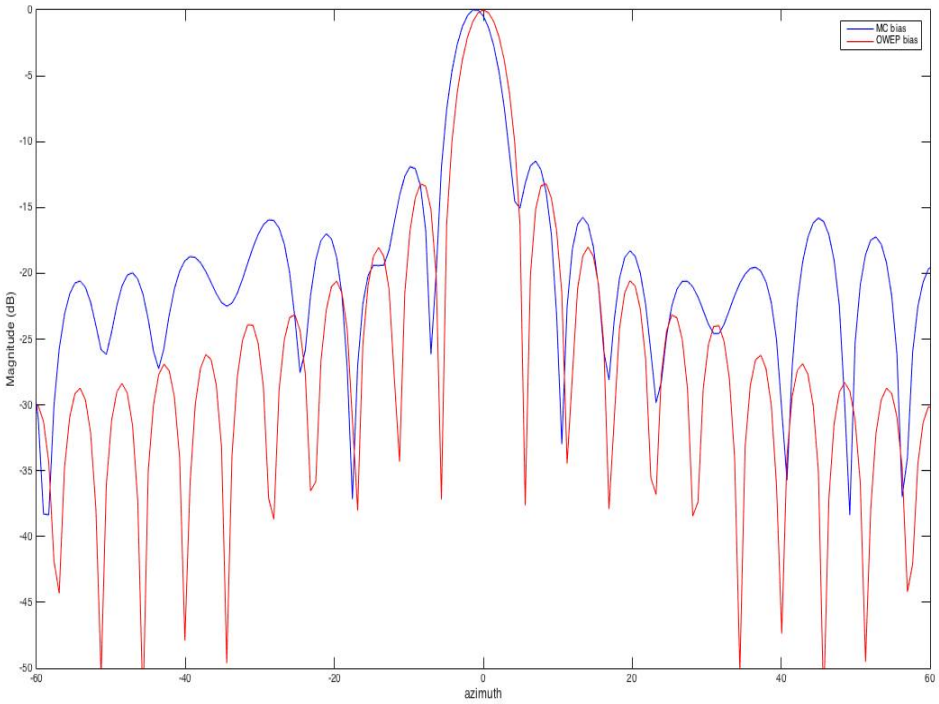

Figure 4.17: Biases introduced by the calibration method and the enviroment.

4.6 Calibrated results

Results after calibration are presented and compared against pre-calibrated measurements. Moreover, ideal settings and applied settings are juxtaposed. As mentioned in section 4.2, co-polar patterns mismatch as well as CPR are the figures of merit used to evaluate the calibration accuracy. Since there is no control over the elevation dimension, the main focus will be on azimuth cut of the array antenna pattern.

Results for a uniform weighting in H port reveal 19 dB improvement after calibration, achieving 38.7 dB CPR. As shown in Figure 4.18, not only is the cross-pol level is reduced over the entire cut, but also the main lobe peak is noticeably reduced. CPR contour plots in Figure 4.19 show that post-calibration results provided at least 15 dB CPR over a wider region along azimuth axis.

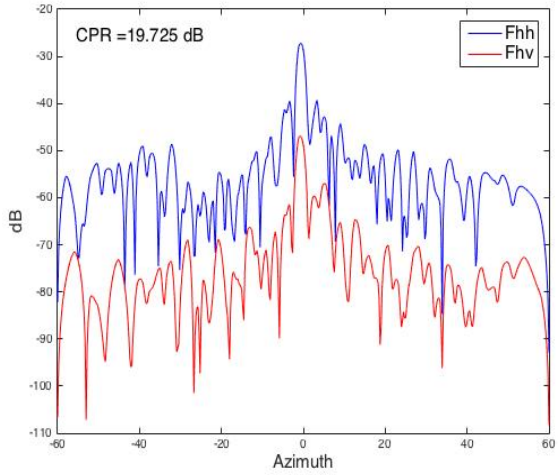

(a) Pre-calibrated

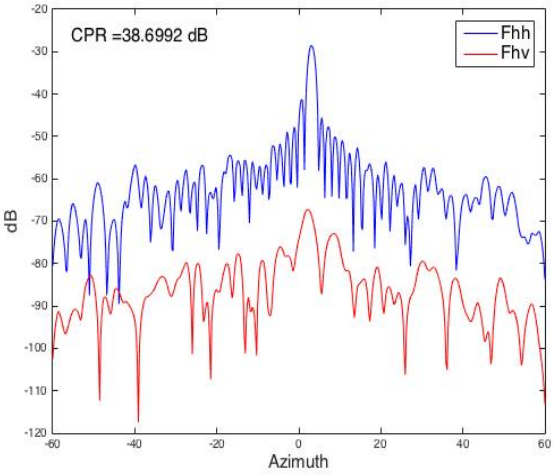

(b) Calibrated

Figure 4.18: Full array co-polar and cross-polar patterns.

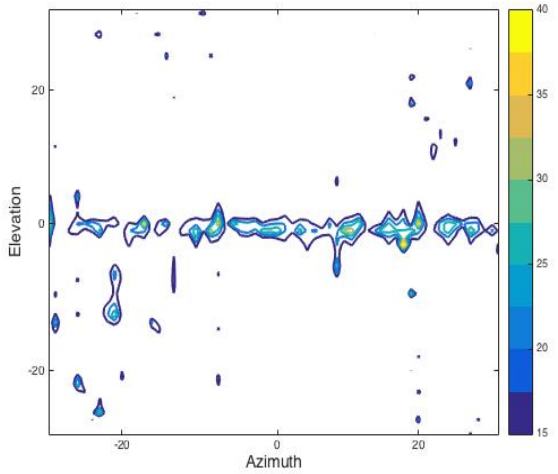

(a) Pre-calibrated

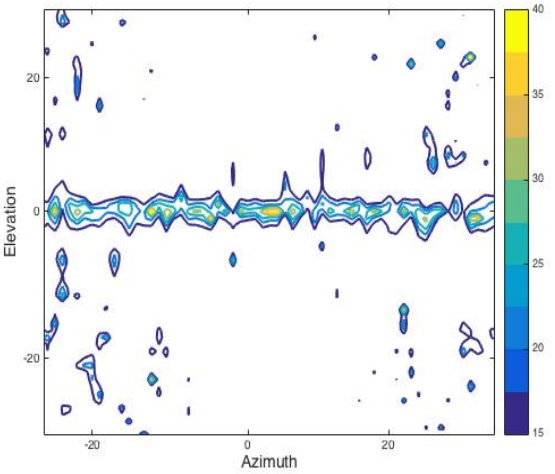

(b) Calibrated

Figure 4.19: CPR contour plots for H polarization.

According to [2], $\arg(\beta_a^2)$ has to be uniform over the beamwidth area for a properly antenna performance. As Figure 4.21b shows, it is flat along 1 degree off the main lobe center, which corresponds to 1.8° of beamwidth. Regarding the Z_{DRb} introduced, less

than 0.1 dB is measured on the center of the main lobe and up to 0.3 dB is introduced over the beamwidth range.

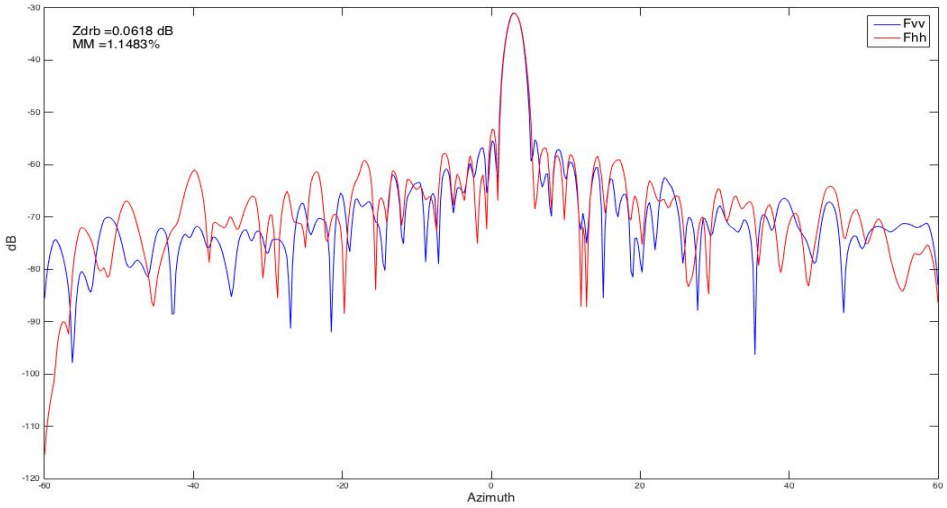

Figure 4.20: Co-polar patern mismatch after calibration, when steered to 3 deg azimuth. MM=1.15% and peak difference of 0.062 dB

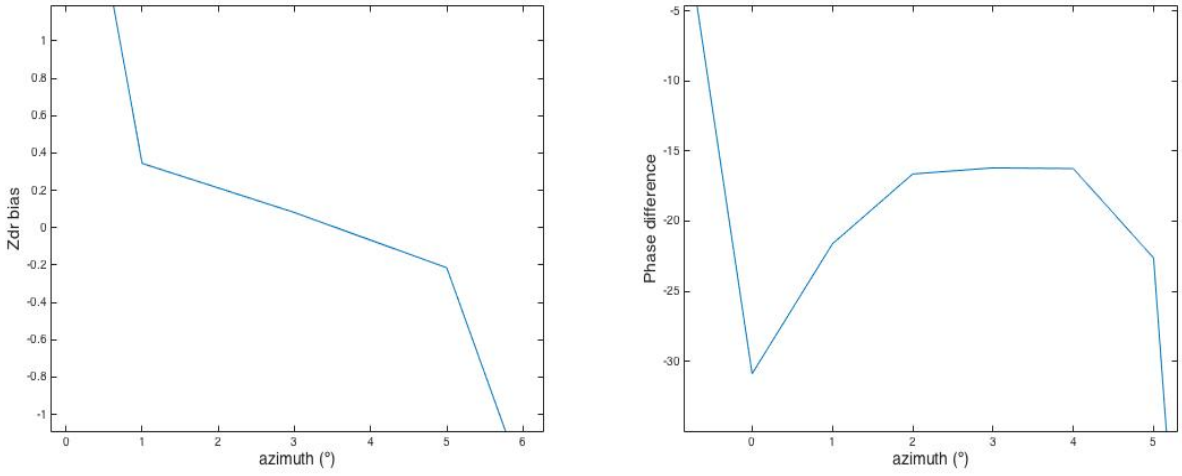

(a) (b)

Figure 4.21: Co-polar patterns mismatch zoom in. Scanning angle is 3° azimuth. Mismatch is represented by β_a^2, squared magnitude expressed as Z_{DRb} in a) and $arg(\beta_a^2)$ expressed as ϕ_{DP} in b).

Ideal and applied settings are shown in Figure 4.22 for a 25 dB Taylor distribution tapering, obtaining up to 9% error that translated in a 0.38 dB amplitude variance. Measured S21 parameter for a given scan angle over all TRMs are set against pre-calibrated results. Ideally, it should be one point with zero phase and magnitude 1, however, errors are expected over the applied settings. This variance can be mitigated by changing the reference value from which settings are computed. As Figure 4.23 shows, it is possible to obtain a better combination of settings.

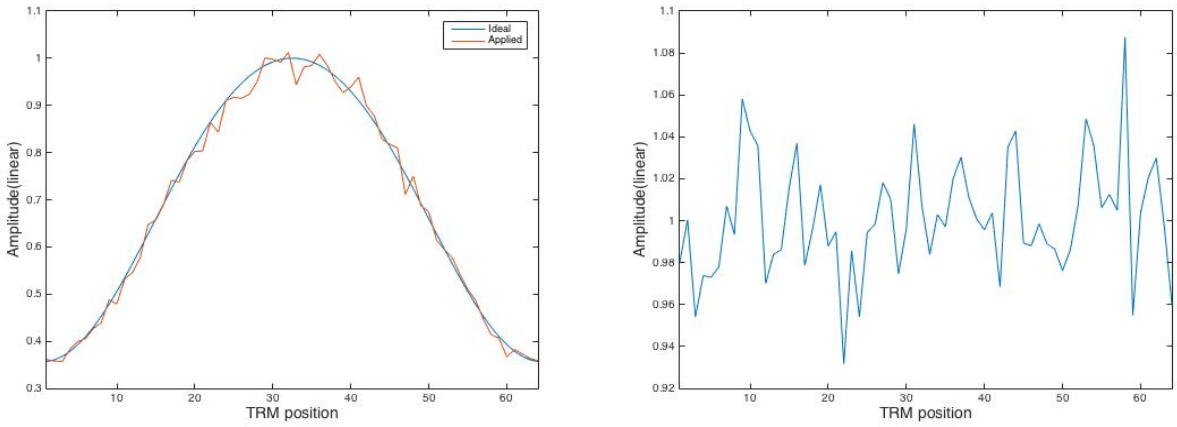

(a) Weighting function: 25 dB sidelobe Taylor distribution

(b) Amplitude error

Figure 4.22: Applied settings differences for a uniform excitation and boresight direction. All values refered to the first TRM.

Finally, broadening as scanned off the broadside can not be corrected by calibration. As explained in section 4.3, the intrinsic element pattern is a constraint over the array pattern. In this case, main lobe peak will be determined by the embedded element shape [9] (see Figure 4.24).

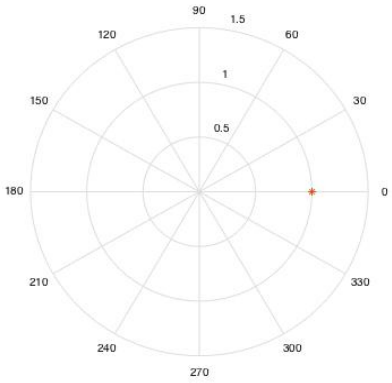

(a) Ideal

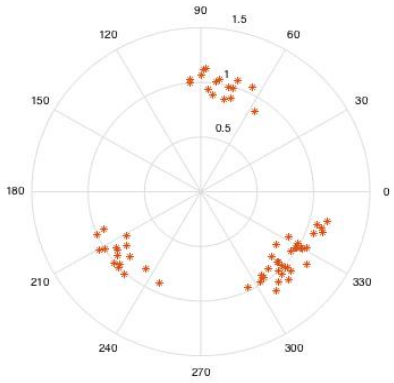

(b) Pre-calibration

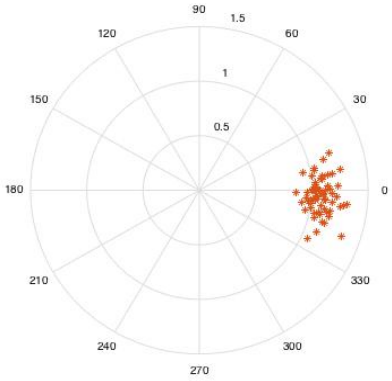

(c) Calibrated

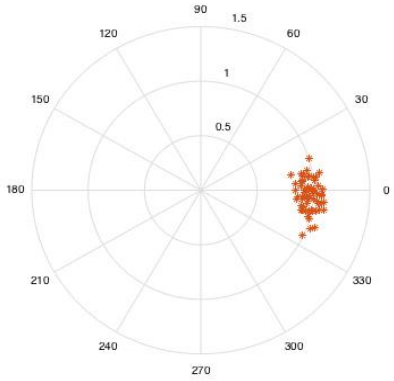

(d) Calibrated using better reference value

Figure 4.23: Applied settings differences for a uniform excitation and boresight direction. All values refered to the first TRM.

$\theta_s(^\circ)$	MM (%)	Z_{DRb}
0	2	0.39 dB
3	4.7	0.06 dB
15	3.6	0.42 dB
30	2.1	0.38 dB
45	-6.5	0.3 dB

Table 4.2: Mismatches in % and bias introduced in Z_{DR} for a steered angle θ_s. Measured beams are 25 dB sidelobe level Taylor distributions.

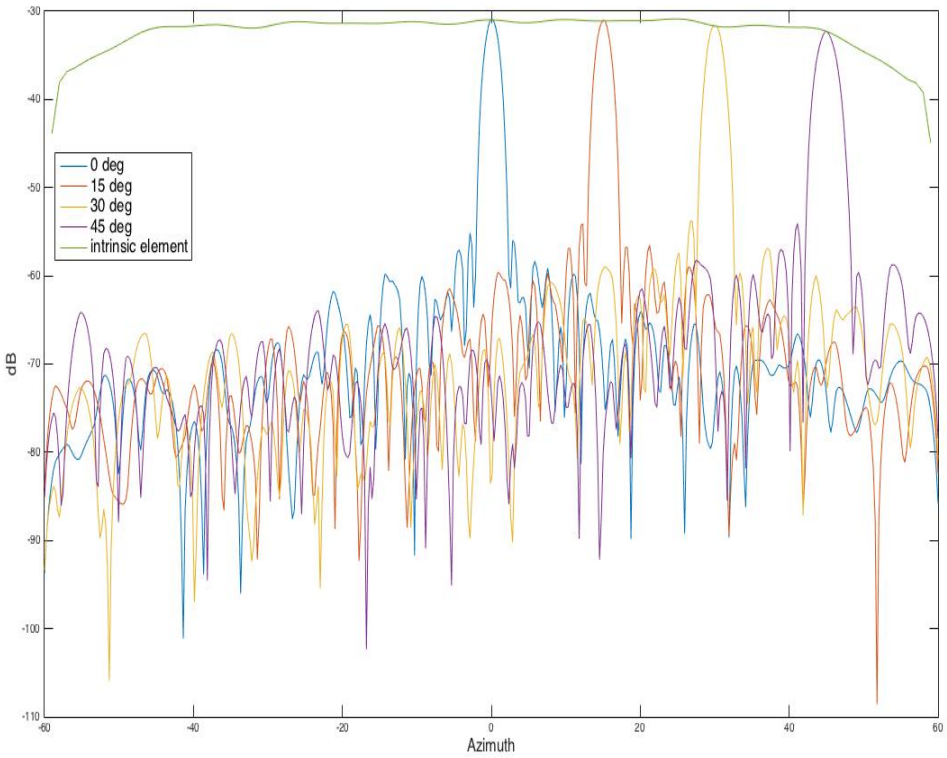

Figure 4.24: Overlapped full array radiation patterns scanning along azimuth, being limited by embedded element pattern shape.

CHAPTER 5

CROSS-POLARIZATION IMPROVEMENT

In remote sensing applications, isolation between polarizations is not just needed on boresight, it is also required along the scan angle range and if possible, over the entire 3D radiation pattern. Integrated Cross-Polarization Ratio (ICPR) measures the isolation levels on more than one point and is defined as:

$$ICPR = -10 \log |\frac{\int F_{cp} F_{xp} \, d\theta}{\int F_{cp}^2 \, d\theta}| \tag{5.1}$$

A novel technique based on sparse arrays described in [10] is tested and appears to improve both CPR and ICPR. This technique will allow to improve these parameters without any hardware modification, once the system is already tested and calibrated.

5.1 Interleaved Sparse Arrays technique for Cross-polarization cancellation

Since PTWR is a one-dimensional scanning array, elevation angle is supposed zero from now on. We divide the antenna into two subsets of elements, each subset has its own array factor, AF_1 and AF_2 respectively. Since the antenna element is not perfect, if port 1 is excited, horizontal and vertical components of the electrical field will be radiated, f_{V1} and f_{H1}, analogous to port 2. One subset is set into one polarization and the other subset is set into the other polarization, thus the two components of the total electric field are:

$$f_{TV} = AF_1 \; f_{V1} + AF_2 \; f_{V2} \tag{5.2}$$

$$f_{TH} = AF_1 \; f_{H1} + AF_2 \; f_{H2} \tag{5.3}$$

where f_{TV} and f_{TH} are the total vertical and horizontal component of the electrical field respectively. And the total radiation pattern can be expressed as:

$$F(\theta, \phi) = |f_{TH}(\theta, \phi)|^2 + |f_{TV}(\theta, \phi)|^2 \tag{5.4}$$

For a given direction, we want to cancel one of the electric field components, in order to improve the cross-polarization. Suppose f_{TH} is the one to be canceled, for a uniformly excited array, being (θ_0, ϕ_0) the boresight direction and using (2.1) and (2.2) definitions, the phase α has to be adjusted to cancel Ψ (see chapter 2). After all this considerations, equation (5.2) becomes:

$$-n_2 \; f_{H2}(\theta_0, \phi_0) = n_1 \; f_{H1}(\theta_0, \phi_0) \tag{5.5}$$

where n_2 and n_1 are the number of elements from each subset. Co-polar and cross-polar phases in each port need to be measured to set such α that cancels Ψ. In summary, H component of the electrical field should be canceled if the proper number of elements are switched (see Figure 5.1). The number of switched elements, called thinning factor, will depend on the CPR value in dB, and is computed as the percentage:

$$K = \frac{1}{1 + 10^{\frac{CPR}{20}}} \tag{5.6}$$

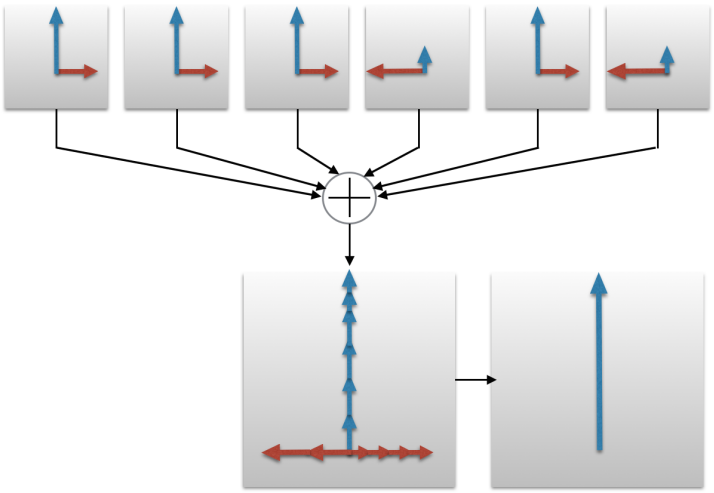

Figure 5.1: Representation for how Interleaved Sparse Arrays works for cross-polarization cancelation.

5.2 Measured results

The main challenge of this technique is working with amplitude and phase steps, because vector cancellation requires precise values. Even with a perfect calibration, steps would not provide all the values from a given span.

A first approach to implement this technique was done using 8 active columns out of 64. That setup, with fewer degrees of freedom, was useful to learn how operate so that experience could be translated to the full array settings.

Figure 5.2 shows the results after applying cross-polarization cancellation. Since this technique tries to cancel one component of the electric field in a given direction, a cross-pol null was expected at that direction. Raw cross-pol has a peak around center of the main lobe, whereas modified pattern has a deep, as expected. Because of the early stage and the phase shifter degree step, patterns had a 2 degree mismatch. 4 dB of CPR improvement is reported if measured at 0 degrees, however, 17 dB of improvement are achieved if measured at the tuned deep angle.

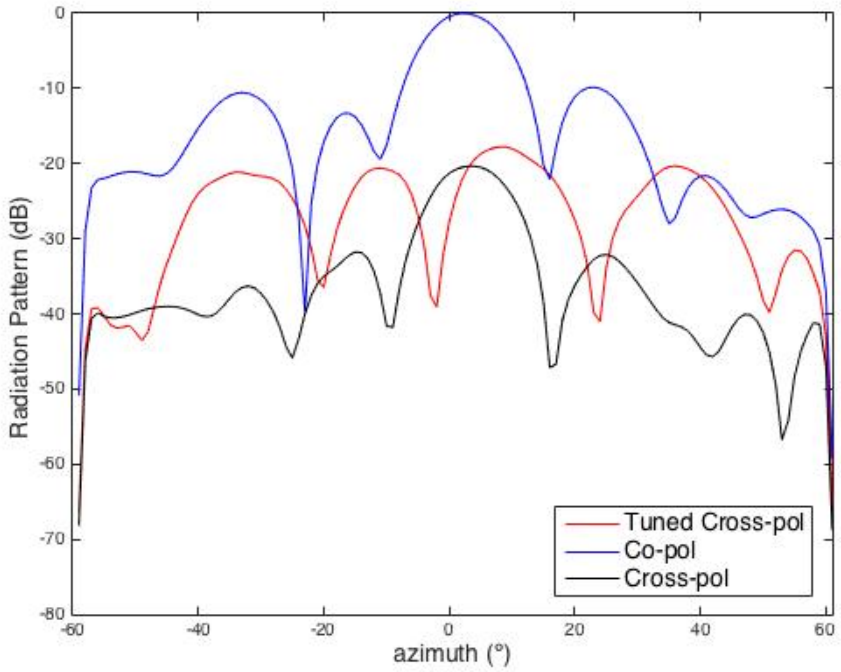

Figure 5.2: Radiation patterns over azimuth cut for a 8 active column array. Co-polar is measured in H port with 1 column switched to V. K=12.5%.

Results using the full array are shown in Figure 5.3, revealing an improvement of 8 dB and 6 dB for CPR and ICPR respectively.

Moreover, a phenomena is observed. Since co-polar power is used to cancel the main lobe peak, the more power received in co-pol, the deeper the peak will be, but on the other hand, higher side-lobe levels will be observed in regions away from the chosen direction because no cancellation is happening there. On that, relies the fact that best on-axis CPR will not imply the best ICPR, therefore, a trade off is needed.

Finally, the repercussions that this technique will imply to the co-polar pattern will be strongly related with the K%. In general, when switching elements, these will not contribute in the co-polar array factor, meaning that a lower and wider main lobe may be observed.

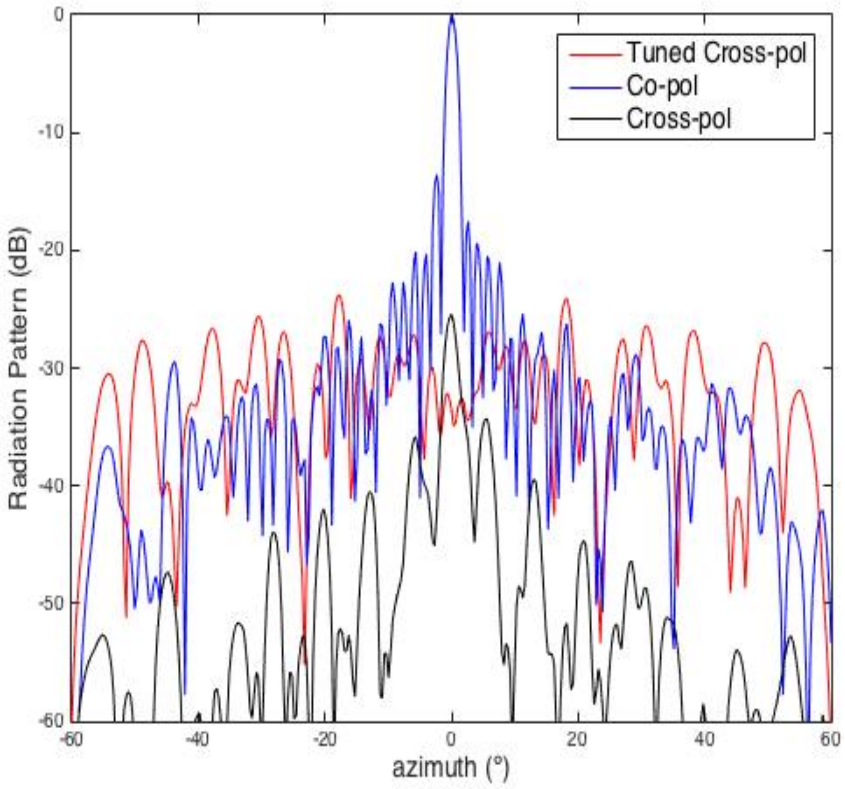

Figure 5.3: Radiation patterns over azimuth cut using all elements. Co-polar is measured in V port, with 4 columns switched to H. K=6.25%.

	8 Columns No cancellation	8 Columns Cancellation	Full Array No cancellation	Full Array Cancellation
CPR	20.6 dB	24.4 dB	25.4 dB	33.6 dB
ICPR(az)	20.4 dB	19.4 dB	25.1 dB	31.2 dB

Table 5.1: CPR and ICPR measured values before and after aplying cross-polarization cancellation over different array settings.

CHAPTER 6

FUTURE WORK

The radar system under study in this thesis revealed poor CPR over elevation cut. Its one-dimension scan does not allow correction for this axis, either for calibration or sparse array techniques. The recently increasing demand and development of dual-pol phased array weather radars for the scientific community leads us to think of a 2D scanning array upgrade. Therefore, cross-polarization cancellation would be completely adjustable and calibration accuracy levels would be much higher because of single element access. On the other hand, another consideration should be the design of a new patch, since as presented in this thesis, the main constraints regarding the cross-polarization rely on the basic element design.

Development of interleaved sparse array algorithms, mainly focused on ICPR improvement would also be needed. As it has been presented, CPR has always had better results. Nonetheless, the study of this technique in transmit mode would also be required, since the major source of cross-polarized signal comes from the transmitter itself. Thus, applying cancellation on both patterns should give much more room of improvement translating to higher data quality.

Finally, taking advantage of the latest set up as a "phased-spin" radar (rotation of array for electronic scanning in elevation), a novel methodology for processing and representing data, presented in [8], could be implemented. The phased-spin setup allows to scan at high elevation angles, up to 30°, obtaining quasi-vertical profiles (QVP) that provide temporal evolution of microphysical processes with high vertical resolution.

APPENDIX A

EXTRA FIGURES

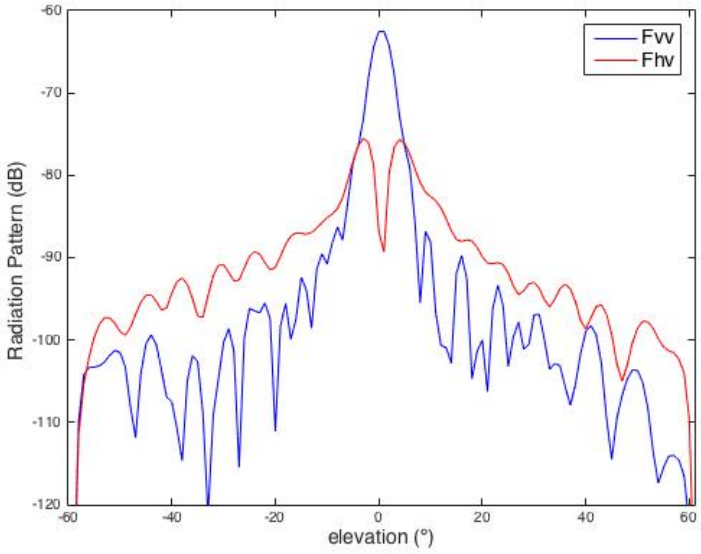

Figure A.1: Unnormalized co-polar and cross-polar column radiation pattern in elevation cut, measured in port V.

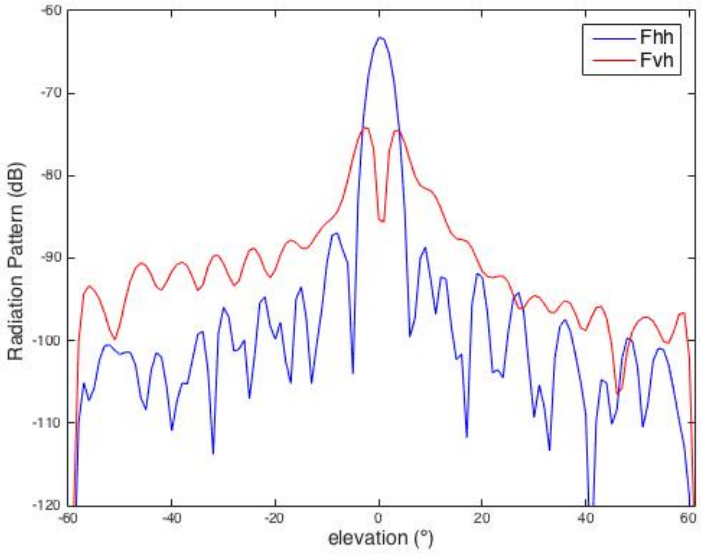

Figure A.2: Unnormalized co-polar and cross-polar column radiation pattern in elevation cut, measured in port H.

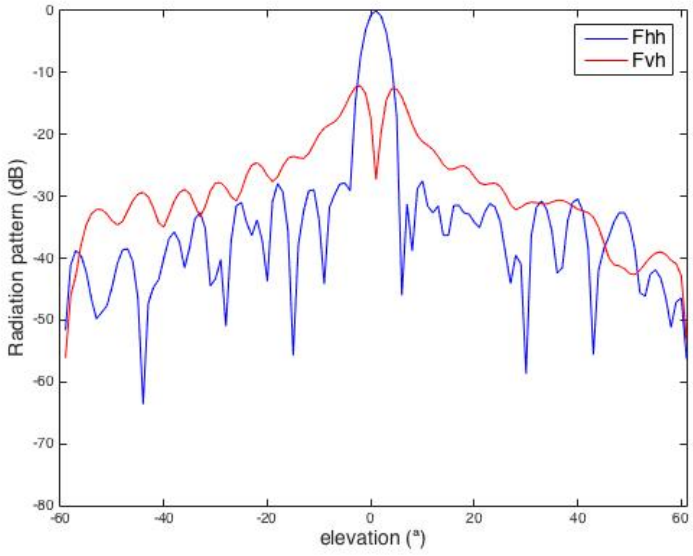

Figure A.3: Co-polar and cross-polar full array radiation pattern in elevation cut, measured in port H.

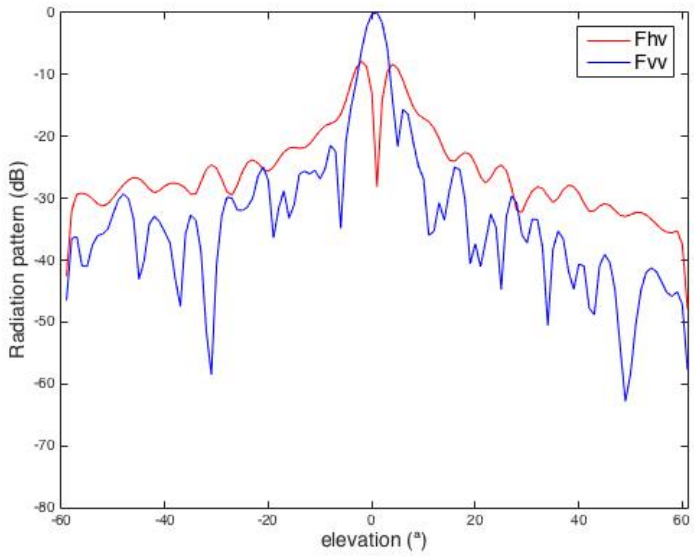

Figure A.4: Co-polar and cross-polar full array radiation pattern in elevation cut, measured in port V.

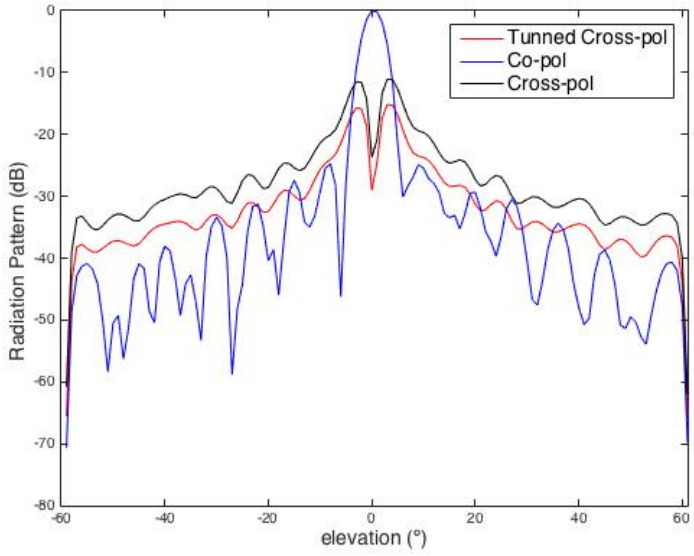

Figure A.5: 8 columns radiation pattern using cross-polarization cancellation. Elevation cut measured in V port.

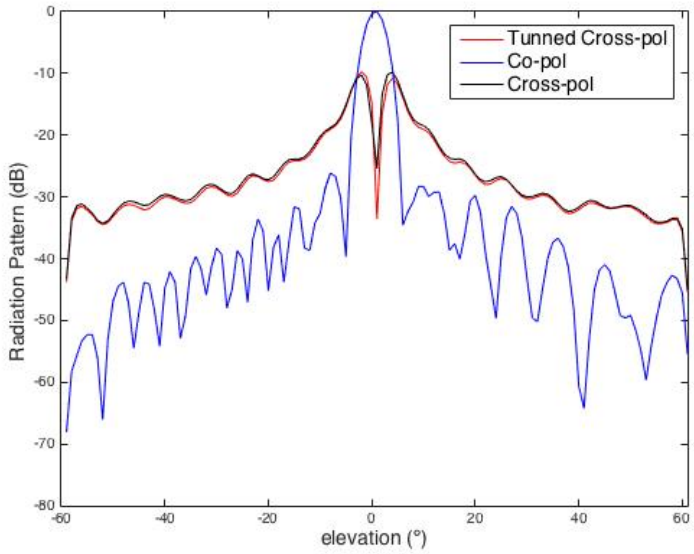

Figure A.6: Full array radiation pattern using cross-polarization cancellation. Elevation cut measured in V port.

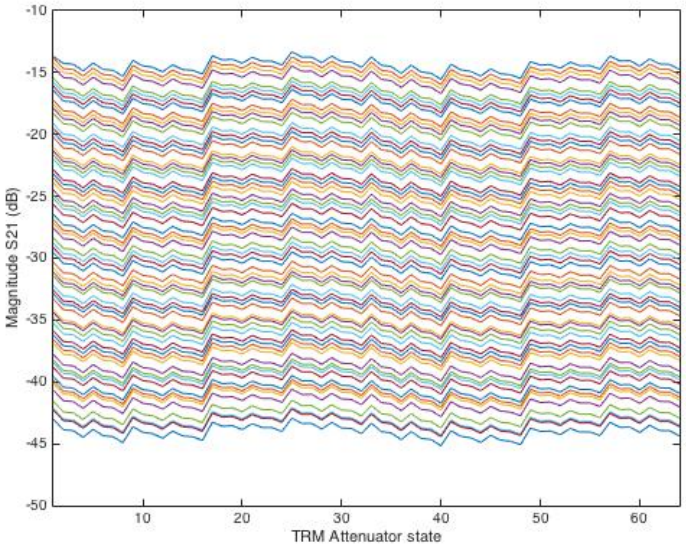

Figure A.7: TRM magnitude of all 4096 states. Measured TRM 1.

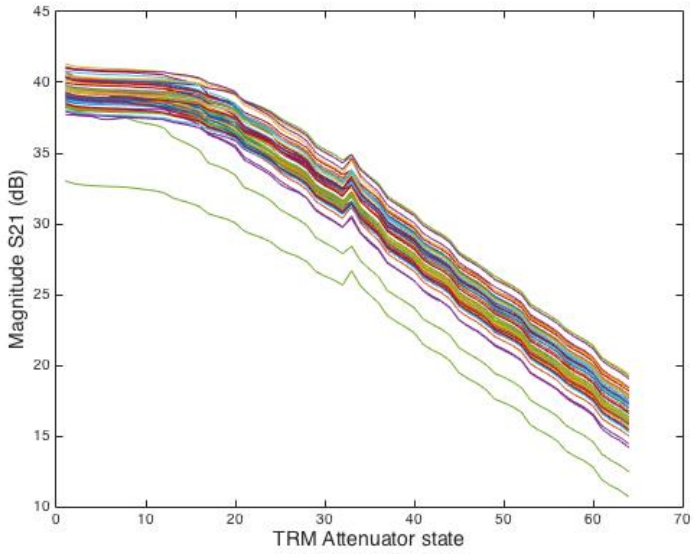

Figure A.8: Magnitude in transmit mode over 64 attenuator levels through 64 TRM. Peak at state 32 is due the TRM register limitation. In order to achieve maximum range the TRM are calibrated to staturate the 10-15 states.

BIBLIOGRAPHY

[1] Aumann, H., A. Fenn, and F. Willwerth (1989), Phased array antenna calibration and pattern prediction using mutual coupling measurements, Antennas and Propagation, IEEE Transactions on, 37 (7), 844-850, doi:10.1109/8.29378.

[2] Bringi, V. N., and V. Chandrasekar (2001), Polarimetric Doppler Weather Radar: Principles and Applications, Cambridge University Press, 6.1, 6.2.

[3] Fulton, C., and W. Chappell (2009), Calibration techniques for digital phased arrays, in Microwaves, Communications, Antennas and Electronics Systems, 2009. COM- CAS 2009. IEEE International Conference on, pp. 1-10, doi:10.1109/COMCAS. 2009.5385979.

[4] Fulton, C., and W. Chappell (2010), Calibration of a Digital Phased Array for Polarimetric Radar, Microwave Symposium Digest (MTT), 2010 IEEE MTT-S International on, 161 - 164, doi:10.1109/MWSYM.2010.5517964

[5] McLaughlin, D., D. Pepyne, V. Chandrasekar, B. Philips, J. Kurose, M. Zink, K. Droegemeier, S. Cruz-Pol, F. Junyent, J. Brotzge, D. Westbrook, N. Bharadwaj, Y. Wang, E. Lyons, K. Hondl, Y. Liu, E. Knapp, M. Xue, A. Hopf, K. Kloesel, A. DeFonzo, P. Kollias, K. Brewster, R. Contreras, B. Dolan, T. Djaferis, E. Insanic, S. Frasier and F. Carr (2009), Short-Wavelenght technology and the potential for distributed networks for small radar systems, Bulletin of the American Meteorological Society, 90(12), 1797-1817, doi:10.1175/2009BAMS2507.1

[6] Medina-Sanchez, Rafael H., Beam steering control system for low-cost phased array weather radars: design and calibration techniques (2013). Doctoral Dissertations 2014-current. Paper 117.

[7] Orzel, Krzysztof, "X-band Dual Polarization Phased-Array Radar for Meteorological Applications" (2015). Doctoral Dissertations 2014-current. Paper 318.

[8] Ryzhkov V. A., P. Zhang, H. D. Reeves, J. Krause, M. R. Kumjian, T. Tschallener, S. Troemel Sr., and C. Simmer, Quasi-vertical profiles - a new concept of examining polarimetric radar data, Extended Abstracts, 37th Conference on Radar Meteorology, American Meteorological Society, Norman, Ok., 5B.2.

[9] Salazar Cerreno, J. L. (2012), The feasibility of low-cost, dual-polarized, phase-tilt antenna arrays for dense radar networks, (Doctoral Dissertation) Available from Proquest.

[10] Sánchez, M., R.W. Jackson, S. Frasier, (2012), Interleaved Sparse Arrays for Polarization Control of Electronically Steered Phased Arrays for Meteorological Applications, IEEE Transactions on Geoscience and Remote Sensing, 50(4), 1283-1290, doi: 10.1109/TGRS.2011.2167016

[11] Wang, Y., and V. Chandrasekar (2006), Polarization isolation requirements for linear dual-polarization weather radar in simultaneous transmission mode of operation, IEEE Transactions on Geoscience and Remote Sensing, 44(8), 2019-2028, doi: 10.1109/TGRS.2006.872138.